NACA RM No. E8K26

RESEARCH MEMORANDUM

EXPERIMENTAL PRESSURE DISTRIBUTIONS OVER WING TIPS AT MACH NUMBER 1.9

I - WING TIP WITH SUBSONIC LEADING EDGE

By James M. Jagger and Harold Mirels

Lewis Flight Propulsion Laboratory
Cleveland, Ohio

NATIONAL ADVISORY COMMITTEE
FOR AERONAUTICS

WASHINGTON
January 27, 1949

NACA RM No. E8K26

NATIONAL ADVISORY COMMITTEE FOR AERONAUTICS

RESEARCH MEMORANDUM

EXPERIMENTAL PRESSURE DISTRIBUTIONS OVER WING TIPS AT MACH NUMBER 1.9

I - WING TIP WITH SUBSONIC LEADING EDGE

By James M. Jagger and Harold Mirels

SUMMARY

An investigation has been conducted at a Mach number of 1.91 to determine the spanwise pressure distribution over a wing tip in the region influenced by a sharp subsonic leading edge swept back at 70°. The supersonic part of the leading edge was normal to the free stream. The wing section was a symmetrical wedge of 5° 43' total included angle in the streamwise direction. The investigation was conducted over a range of angles of attack from -16° to 16°.

The experimental data were in good agreement with linearized theory for small angles of attack, but the difference between theory and experiment increased with angle of attack. Except for the pressure distribution on the top surface in the immediate vicinity of the subsonic leading edge, the maximum difference (expressed as a percentage of free-stream dynamic pressure) was $2\frac{1}{2}$ percent for angles of attack up to 4° and 7 percent for angles of attack up to 8°. The pressures on the top surface nearest the subsonic edge indicated local expansions beyond the values predicted by linearized theory. The bottom surface in this region, however, continued to agree fairly closely with linearized theory. Where consideration of the Mach number on the wing surface indicated that a pressure orifice was in the two-dimensional-flow region, the agreement between exact two-dimensional theory and the experimental data was generally excellent.

INTRODUCTION

Linearized solutions for the pressure distribution over thin supersonic wings have been presented in numerous papers (for example, references 1 to 5). These derivations assume nonviscous flow and

small perturbation velocities. The applicability of these assumptions to a real fluid flowing past a wing of finite thickness can be determined only by experiment. Relatively few investigations have been reported that compare experimental pressure distributions over three-dimensional wings with those predicted by linearized theory. An investigation of a 63° swept airfoil of biconvex section is presented in references 6 and 7. Close agreement between theory and experiment was obtained for all regions except those influenced by the subsonic trailing edge and the tip.

Results of the first part of an investigation conducted at the NACA Lewis laboratory to determine pressure distributions in those regions of a three-dimensional wing where the use of linearized theory may be questionable are presented herein. Experimental pressures and the resulting load distribution in the neighborhood of a sharp subsonic leading edge (along which linearized theory predicts infinite pressures) are compared with theory.

SYMBOLS

The following symbols are used in this report:

C_p	pressure coefficient, $(p-p_0)/q_0$
K	constant whose value is $\frac{1+\beta_0 \cot \theta}{1-\beta_0 \cot \theta}$
M_0	free-stream Mach number
M_1	Mach number on surface of wing in two-dimensional region
p	local static pressure on wing surface
p_0	free-stream static pressure
p_{ex}	static pressure determined from experiment
p_{th}	static pressure predicted by linearized theory
q_0	free-stream dynamic pressure, $\frac{1}{2}\rho_0 U^2$
U	free-stream velocity
x,y	Cartesian coordinates

[redacted]

α angle of attack measured between chord line and free-stream direction

$\beta_0 = \sqrt{M_0^2-1}$

$\beta_1 = \sqrt{M_1^2-1}$

$\beta_0 y/x$ conical coordinate

θ angle of sweepback of subsonic edge

ρ_0 free-stream static density

σ half wedge angle measured in y = constant planes (slope)

φ perturbation velocity potential

Subscripts:

B bottom wing surface

T top wing surface

APPARATUS AND PROCEDURE

The investigation was conducted in the Lewis 18- by 18-inch supersonic tunnel. From a previous calibration, the Mach number in the vicinity of the wing was determined to be 1.91 with a maximum variation of $\pm 1/2$ percent. The Reynolds number was 3.4×10^6 per foot.

A photograph of the wing model installed in the tunnel is shown in figure 1. The model was mounted on a sweptback strut. The angle of attack was varied by changing the angle of the strut with respect to the air stream and was read on a vernier scale to an accuracy of $\pm 2\frac{1}{2}$ minutes.

A sketch of the wing model showing the principle dimensions is presented in figure 2. The forward wing section, in which the orifices were located, was a symmetrical wedge with an included angle of 5° 43' in the free-stream direction. The supersonic leading edge was normal to the air stream and the subsonic leading edge was swept back at an angle of 70°

The model was machined from two pieces of tool steel; the rear section was a fairing to decrease the magnitude of the disturbances toward the rear of the model. The leading edges were straight and were ground to knife edges. After instrumentation had been installed, the two pieces of the wing were fastened together and the entire model was finish-ground.

The location of the static-pressure orifices is shown in figure 2. The orifices were 0.010 inch in diameter, sharp-edged, and free of burs. Pressures were photographically recorded on a multiple-tube manometer board using tetrabromomethane as the manometer fluid.

THEORY

The pressure coefficient on the surface of the wing at angle of attack can be expressed, according to linearized theory, as

$$C_p = C_p(\sigma) + C_p(\alpha) \tag{1}$$

where

$C_p(\sigma)$ pressure coefficient on surface of given wing at zero angle of attack

$C_p(\alpha)$ pressure coefficient on surface of flat plate, of given plan form, at angle of attack

These pressure coefficients can be derived from the perturbation velocity potential.

The potential in the three-dimensional flow region $(-1<\beta_0 y/x<1)$ for the wing at zero angle of attack, obtained from reference 5, is

$$\varphi_T(\sigma) = \frac{U\sigma}{\pi\beta_0}\left[-2x \tan^{-1}\sqrt{\frac{x-\beta_0 y}{x+\beta_0 y}} + \frac{(K-1)x-(K+1)\beta_0 y}{\sqrt{K}} \log_e \frac{\sqrt{(K-1)x-(K+1)\beta_0 y}}{\sqrt{K(x-\beta_0 y)}+\sqrt{x+\beta_0 y}}\right]$$

[redacted]

The coordinate system is illustrated in figure 2. The corresponding pressure coefficient is then

$$C_{p,T}(\sigma) = -\frac{2}{U}\frac{\partial \varphi_T(\sigma)}{\partial x}$$

$$= \frac{-2\sigma}{\pi\beta_0}\left[\frac{(K-1)}{\sqrt{K}}\log_e \frac{\sqrt{K\left(1-\frac{\beta_0 y}{x}\right)}-\left(1+\frac{\beta_0 y}{x}\right)}{\sqrt{K\left(1-\frac{\beta_0 y}{x}\right)}+\sqrt{1+\frac{\beta_0 y}{x}}} - 2\tan^{-1}\sqrt{\frac{1-\frac{\beta_0 y}{x}}{1+\frac{\beta_0 y}{x}}}\right] \tag{2}$$

The flow is conical, as evidenced by the fact that the pressure coefficient depends only on $\beta_0 y/x$. The linearized pressure coefficient for the two-dimensional region $\beta_0 y/x \leq -1$ is obtained by setting $\beta_0 y/x = -1$ and yields

$$C_{p,T}(\sigma) = 2\sigma/\beta_0 \tag{3}$$

The pressure distribution is identical for the top and bottom surfaces of a symmetrical wing at zero angle of attack; thus

$$C_{p,T}(\sigma) = C_{p,B}(\sigma) \tag{4}$$

The perturbation velocity potential in the three-dimensional-flow region of the flat-plate wing, also obtained from reference 5, is

$$\varphi_T(\alpha) = \frac{U\alpha}{\pi\beta_0}\left[\sqrt{\frac{(K+1)(x+\beta_0 y)\left[(K-1)x-(K+1)\beta_0 y\right]}{K^2}}\right.$$

$$\left. + 2x\tan^{-1}\sqrt{\frac{(K-1)x-(K+1)\beta_0 y}{(K+1)(x+\beta_0 y)}}\right]$$

The corresponding pressure coefficient is then

$$C_{p,T}(\alpha) = \frac{-2\alpha}{\pi\beta_0}\left[2\tan^{-1}\sqrt{\frac{K\left(1-\frac{\beta_0 y}{x}\right)-\left(1+\frac{\beta_0 y}{x}\right)}{(K+1)\left(1+\frac{\beta_0 y}{x}\right)}}\right.$$

$$\left.+\left(\frac{K-1}{K}\right)\sqrt{\frac{(K+1)\left(1+\frac{\beta_0 y}{x}\right)}{K\left(1-\frac{\beta_0 y}{x}\right)-\left(1+\frac{\beta_0 y}{x}\right)}}\right] \qquad (5)$$

For the two-dimensional region, this expression reduces to

$$C_{p,T}(\alpha) = -2\alpha/\beta_0 \qquad (6)$$

The pressure distribution on the bottom surface of a flat-plate wing is the negative of that for the top surface, or

$$C_{p,T}(\alpha) = -C_{p,B}(\alpha) \qquad (7)$$

Equations (1) to (7) completely define the linearized pressure distribution for the experimental wing model.

The flow in the two-dimensional region is equivalent to flow about a wedge. A nonviscous fluid solution, herein designated the exact two-dimensional solution, is available from the oblique shock and Prandtl-Meyer relations (reference 8).

Linearized theory, which assumes a constant Mach number throughout the flow field, defines the two-dimensional region as $\beta_0 y/x \leq -1$. A more accurate definition is $\beta_1 y/x \leq -1$, where β_1 is determined from the exact two-dimensional solution for flow about the wedge. Thus an orifice in the neighborhood of $\beta_0 y/x = -1$ may be in either the two- or three-dimensional flow region, depending on the angle of attack. With increasing positive angles of attack, the effective area of the two-dimensional region increases on the top surface and decreases on the bottom surface.

RESULTS AND DISCUSSION

The wing model was investigated over the range of angles of attack from -16° to 16°. Because of wing symmetry, the pressures

on one surface at a positive angle of attack should equal the pressures on the opposite surface at the same negative angle of attack. The experimental data for both positive and negative angles of attack are therefore presented in figures 3 to 6 to correspond to the top and bottom surfaces of the wing through the positive-angle-of-attack range. Schlieren photographs indicated that after the wing had been turned beyond an angle of 10°, the shock wave was detached from the sweptback support strut and influenced the pressure orifices on the bottom wing surface, which made the data unreliable. Because the detached shock wave had no apparent effect on the top-wing-surface pressures, data are presented up to an angle of attack of 16° for this surface.

Pressure Distributions

Vicinity of two-dimensional-flow region. - The experimental variation of pressure coefficient at orifice station $\beta_0 y/x = -1.27$ is compared with both linearized and exact theory in figure 3(a). The experimental data are in excellent agreement with the exact theory for the entire range. Linearized theory shows very good agreement for the top surface in the neighborhood of the angle at which the top surface is parallel to the flow ($\alpha = 2^\circ 52'$). With changes in angle of attack from the parallel-flow condition, linearized theory and the experimental data diverge continuously.

The results for stations $\beta_0 y/x = -1.07$, -0.91, and -0.77 are presented in figures 3(b) to 3(d). The angles of attack for which each orifice was in the two-dimensional region ($\beta_1 y/x \leq -1$) are noted in these figures. The agreement between experiment and exact two-dimensional theory is generally excellent in this range. The divergence between experiment and the exact theory is seen to occur when the orifice is well within the three-dimensional-flow region. A similar effect of local wing Mach number is noted in reference 6. The effect of the tip, as predicted by linearized theory, is to diminish the magnitude of the pressures below those existing in the two-dimensional region.

Center of three-dimensional-flow region. - Linearized theory and experiment are compared in figures 3(e) to 3(i) for stations well within the three-dimensional-flow region. Close agreement for angles of attack involving small surface deflections, and the characteristic divergence between experiment and theory with increasing angle of attack, are again evident.

Vicinity of subsonic leading edge. - The experimental data obtained from orifices in the immediate vicinity of the subsonic

leading edge are presented in figures 3(j) to 3(l). The first severe departure from linearized theory, a rapid decrease with angle of attack in the pressure coefficient for the top surface, is shown in these figures. This discrepancy can be accounted for by consideration of the flow in the neighborhood of the subsonic edge. In this region, the local deflections undergone by the component of the flow parallel to the edge are negligible compared with those undergone by the normal component of flow. The pressure distribution in this region is therefore comparable to that for a sharp-edged airfoil at a high subsonic Mach number. (The total included wedge angle measured normal to the subsonic edge is $16\frac{2}{3}^\circ$ for the experimental model; the normal Mach number is 0.65.) In the investigation of such airfoils discussed in reference 9, an expansion around the edge of the type encountered in supersonic flow was observed, which terminated in an oblique shock; no separation was noted.

A plot of the spanwise pressure distribution on the top surface is presented in figure 4 for three representative angles of attack. At a 4° angle of attack, the data from stations $\beta_0 y/x = 0.47$ and $\beta_0 y/x = 0.43$ indicate a rapid compression, but the pressure coefficients at these stations are considerably lower than those predicted by linearized theory because of the expansion around the subsonic edge. The curve for the 8° angle of attack indicates that expansion continues to station $\beta_0 y/x = 0.43$ and then a rapid compression occurs. This compression may be associated with an oblique shock. At the 14° angle of attack the expansion continues until $\beta_0 y/x = 0.30$ before the compression occurs.

The sharp drop in pressures on the top wing surface observed in figures 3(j) to 3(l) can thus be attributed to a local expansion of the normal flow about the subsonic edge. The severity and extent of the expansion region increased with angle of attack. The analogy between the subsonic leading edge and a sharp-edged airfoil in subsonic flight indicates that no unusual flow phenomenon is to be expected on the bottom surface. The pressures on the bottom surface agreed fairly closely with linearized theory for those stations.

Differences between Linearized Theory and Experiment

The applicability of linearized theory for determining the pressure distribution on the given wing configuration is illustrated in figure 5 where the difference between the experimental data and the

predictions of linearized theory is presented as a percentage of free-stream dynamic pressure. The curves for orifices in the range $-1.27 \leqq \beta_0 y/x \leqq 0.16$ are similar and follow the characteristic trend of increasing divergence between linearized theory and experiment with increasing angles of attack. The limiting curves ($\beta_0 y/x = -1.27$ and 0.16) for this range are shown in figure 5. The maximum difference is $2\frac{1}{2}$ percent for angles of attack up to 4° and 7 percent for angles of attack up to 8°. For the stations near the edge ($0.30 \leqq \beta_0 y/x \leqq 0.47$), the observed difference for the top surface reached a maximum magnitude of $15\frac{1}{2}$ percent. The difference for the bottom surface in this region, however, did not exceed 4 percent.

Load Distribution

Experimental values of load coefficient, expressed in parameter form, are compared with linearized theory in figure 6. The experimental values are generally higher than the theoretical. Stations nearest the subsonic edge show the largest disagreement. The disagreement is associated with the low pressures on the top surface in this region.

SUMMARY OF RESULTS

An investigation has been conducted at a Mach number of 1.91 to determine the spanwise pressure distribution in the tip region of a wing having a sharp subsonic leading edge.

The experimental data were in close agreement with linearized theory for the range of angles of attack close to that at which the airfoil surface is parallel to the free-stream direction. Experiment and linearized theory diverged continuously with increasing angle of attack. Except for stations in the immediate vicinity of the subsonic leading edge, the maximum difference (expressed as a percentage of free-stream dynamic pressure) was $2\frac{1}{2}$ percent for angles of attack up to 4° and 7 percent for angles of attack up to 8°. For stations on the top surface nearest the subsonic edge, local expansions beyond the values predicted by linearized theory were indicated and the maximum observed discrepancy was $15\frac{1}{2}$ percent. The bottom surface in this region, however, continued to agree

fairly closely with linearized theory. Where consideration of the Mach number on the wing surface indicated that a pressure orifice was in the two-dimensional flow region, the agreement between exact two-dimensional theory and the experimental data was generally excellent.

Lewis Flight Propulsion Laboratory,
National Advisory Committee for Aeronautics,
Cleveland, Ohio.

REFERENCES

1. Puckett, Allan E.: Supersonic Wave Drag of Thin Airfoils. Jour. Aero. Sci., vol. 13, no. 9, Sept. 1946, pp. 475-484.

2. Jones, Robert T.: Thin Oblique Airfoils at Supersonic Speed. NACA Rep. No. 851, 1946.

3. Stewart, H. J.: The Lift of a Delta Wing at Supersonic Speeds. Quarterly Appl. Math., vol. IV, no. 3, Oct. 1946, pp. 246-254.

4. Brown, Clinton E.: Theoretical Lift and Drag of Thin Triangular Wings at Supersonic Speeds. NACA Rep. No. 839, 1946.

5. Evvard, John C.: Distribution of Wave Drag and Lift in the Vicinity of Wing Tips at Supersonic Speeds. NACA TN No. 1382, 1947.

6. Frick, Charles W., and Boyd, John W.: Investigation at Supersonic Speed (M = 1.53) of the Pressure Distribution over a 63° Swept Airfoil of Biconvex Section at Zero Lift. NACA RM No. A8C22, 1948.

7. Boyd, John W., Katzen, Elliott D., and Frick, Charles W.: Investigation at Supersonic Speed (M = 1.53) of the Pressure Distribution over a 63° Swept Airfoil of Biconvex Section at Angles of Attack. NACA RM No. A8F22, 1948.

8. The Staff of the Ames 1- by 3-Foot Supersonic Wind-Tunnel Section: Notes and Tables for Use in the Analysis of Supersonic Flow. NACA TN No. 1428, 1947.

9. Lindsey, W. F., Daley, Bernard N., and Humphreys, Milton D.: The Flow and Force Characteristics of Supersonic Airfoils at High Subsonic Speeds. NACA TN No. 1211, 1947.

[redacted]

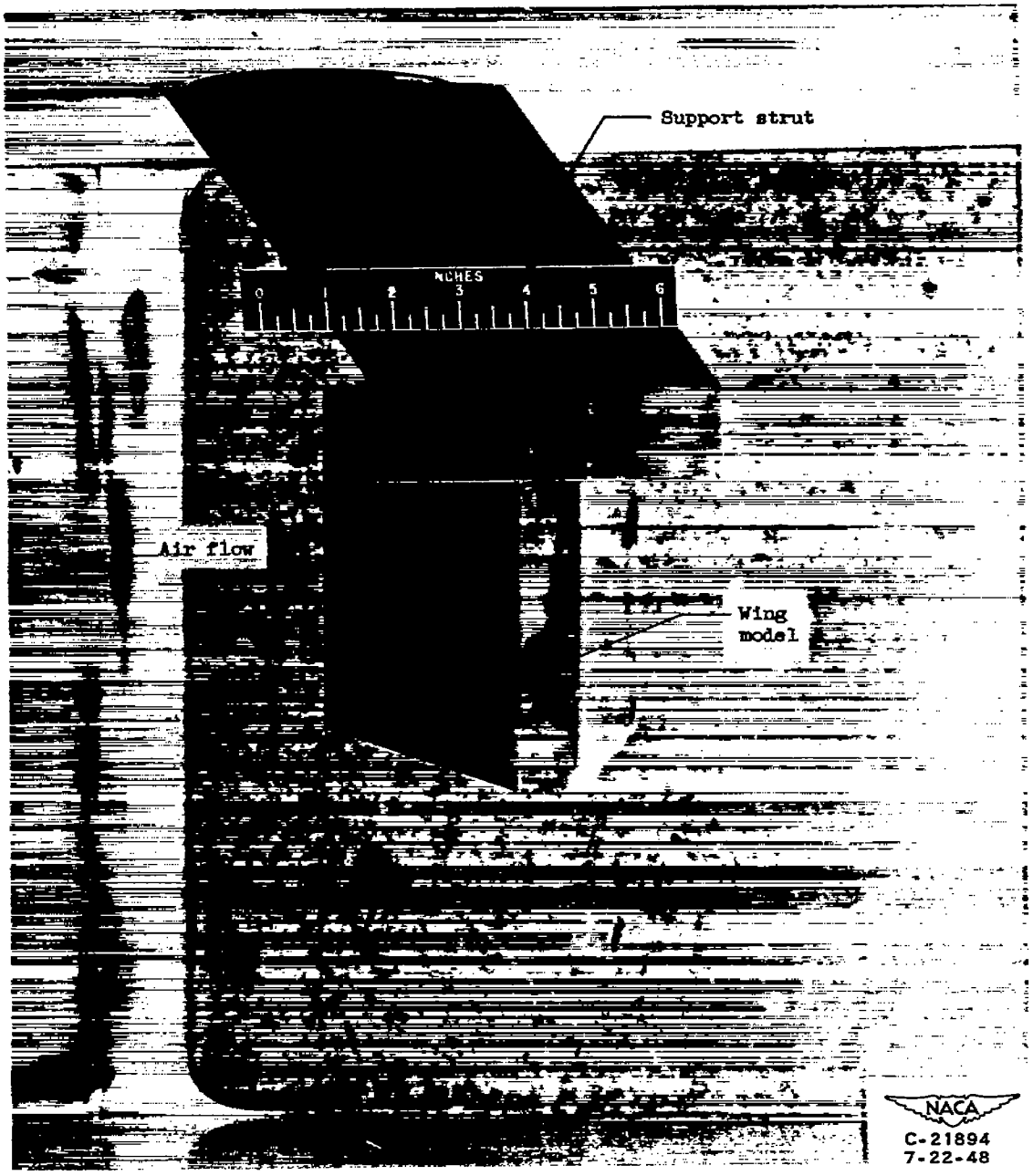

Figure 1. - Installation of wing model in 18- by 18-inch supersonic tunnel.

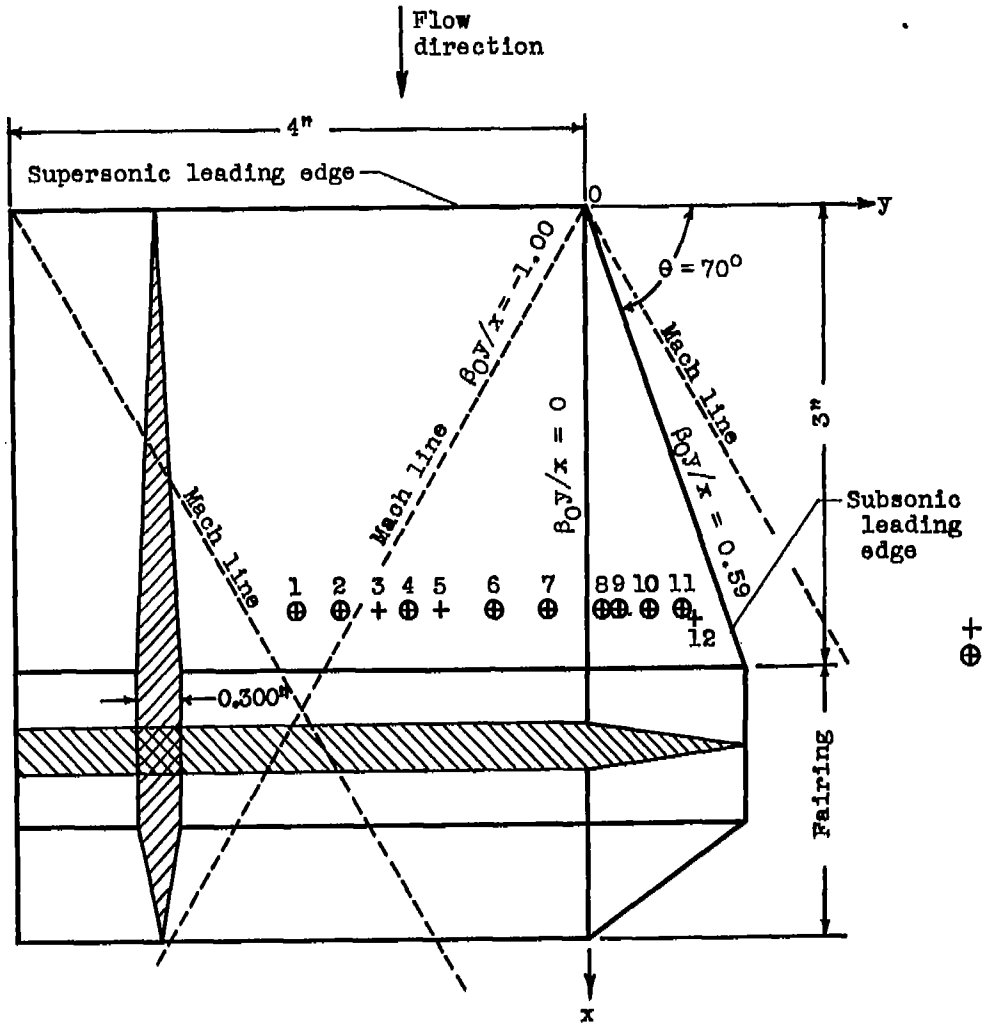

Orifice	$\beta_0 y/x$
1	-1.27
2	-1.07
3	-.91
4	-.77
5	-.63
6	-.40
7	-.16
8	.08
9	.16
10	.30
11	.43
12	.47

\+ Orifice on one surface
⊕ Orifice on both surfaces

NACA

Figure 2. - Sketch of wing-tip model showing principal dimensions and locations of pressure orifices.

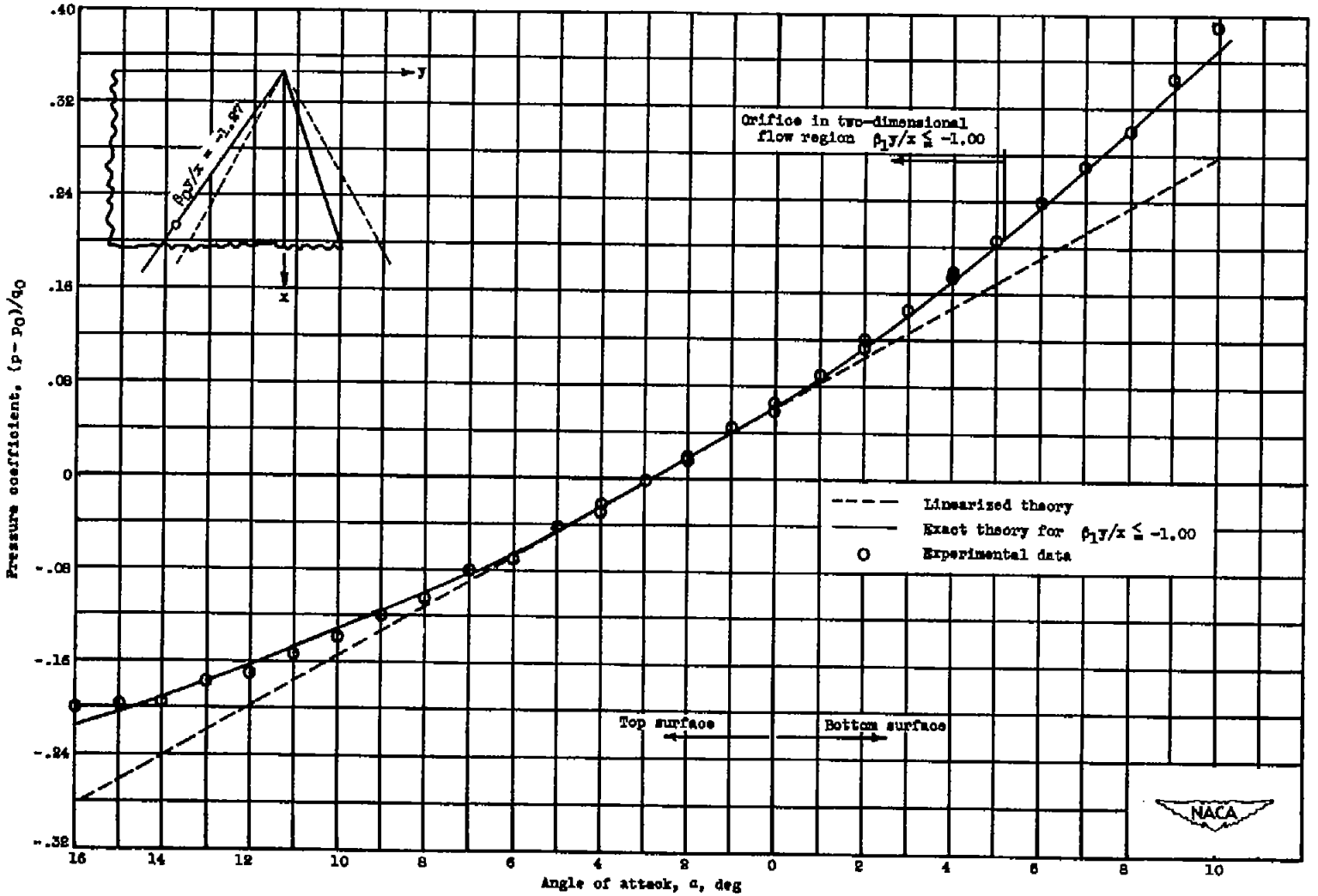

(a) $\beta_0 y/x = -1.27$.

Figure 3. - Variation of pressure coefficient with angle of attack at each orifice station.

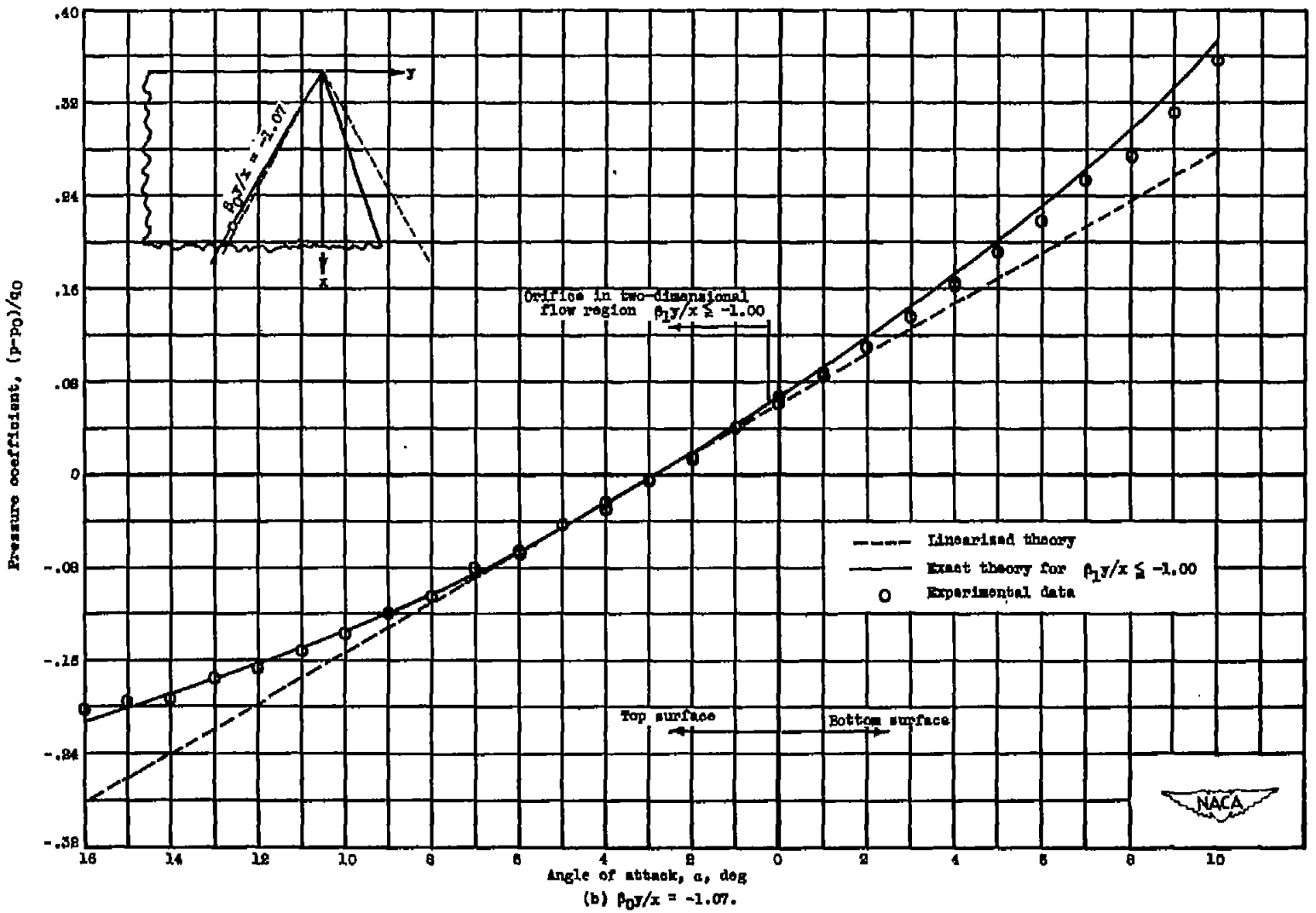

(b) $\beta_0 y/x = -1.07$.

Figure 3. - Continued. Variation of pressure coefficient with angle of attack at each orifice station.

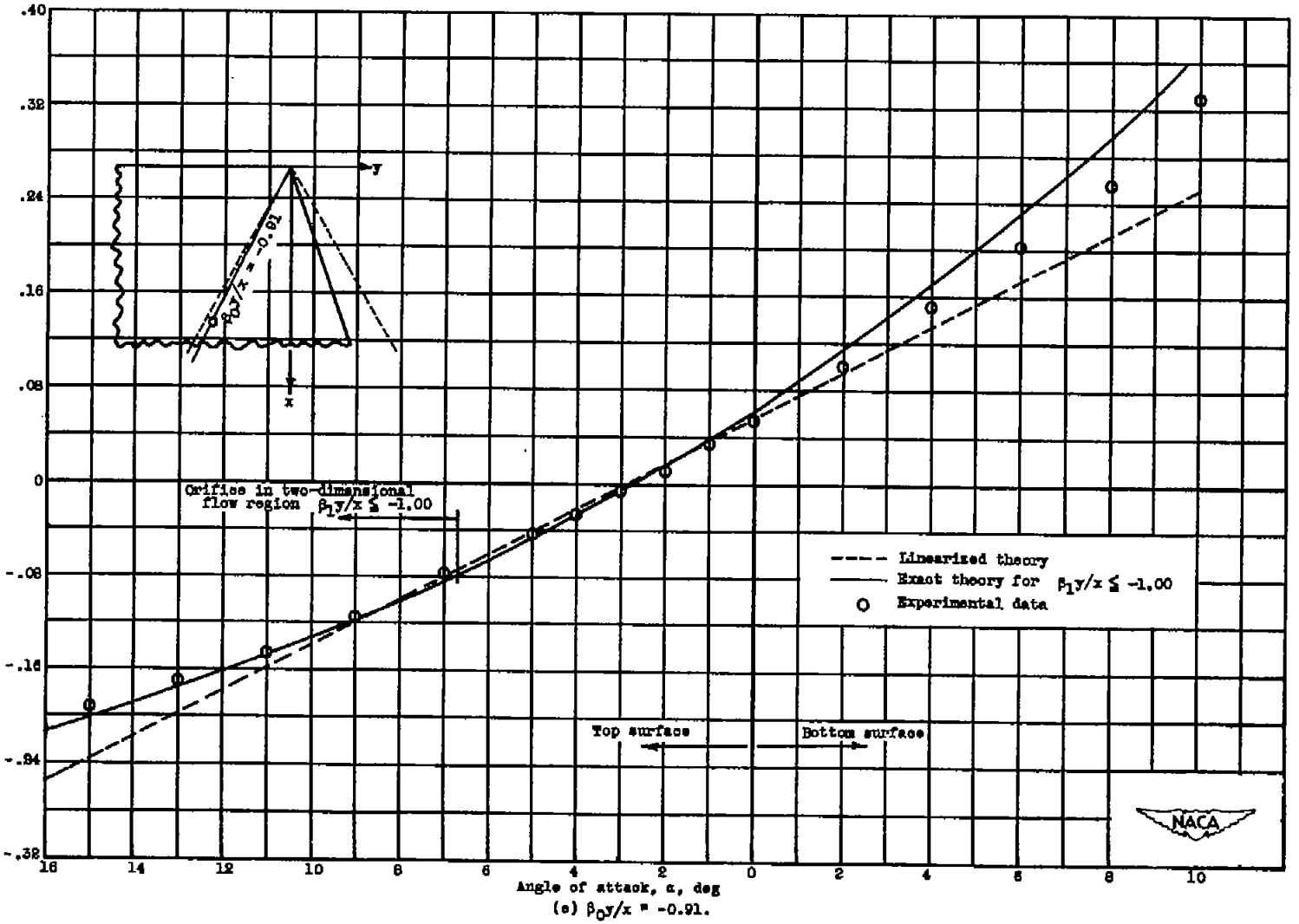

(e) $\beta_0 y/x = -0.91$.

Figure 3. - Continued. Variation of pressure coefficient with angle of attack at each orifice station.

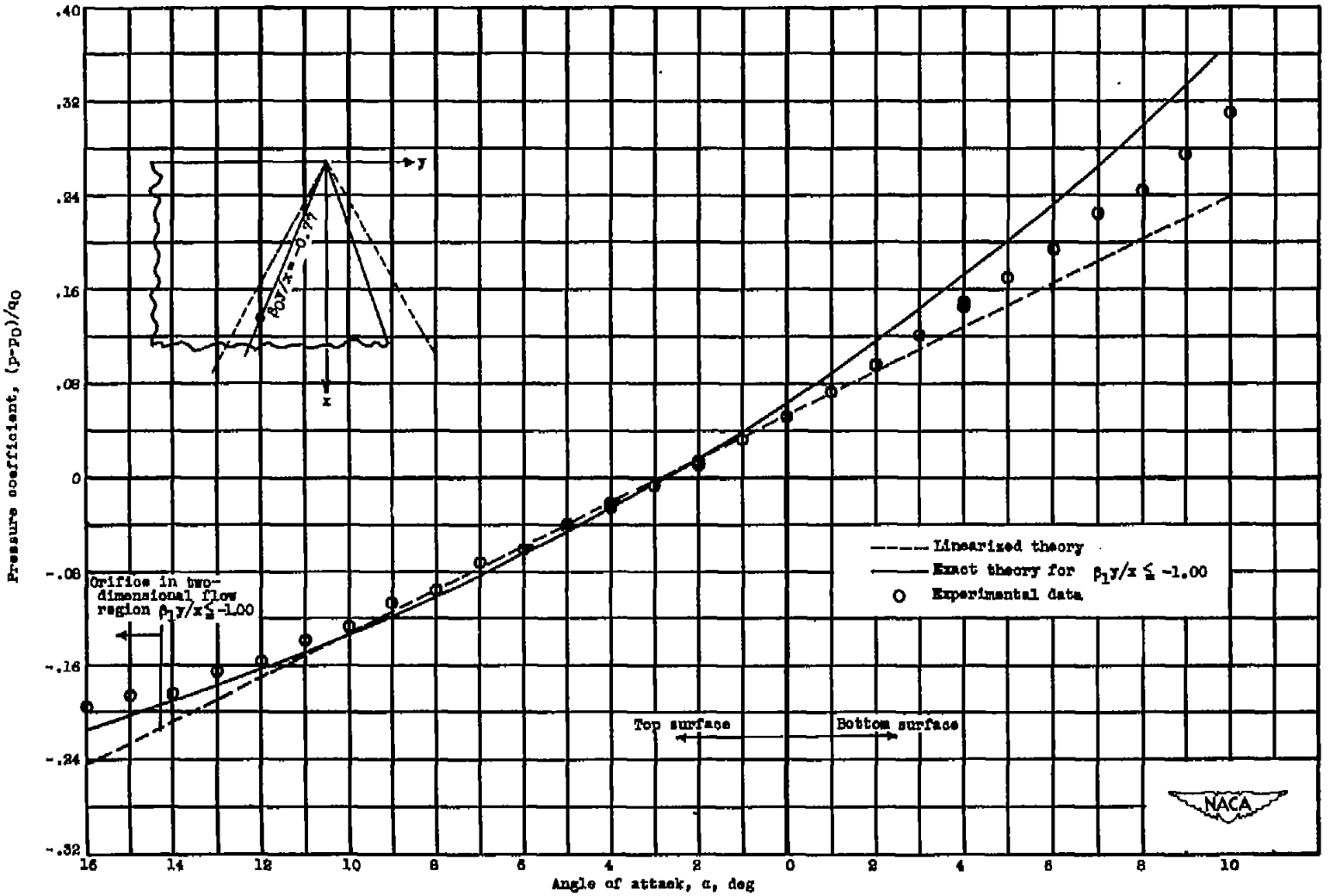

(d) $\beta_0 y/x = -0.77$.

Figure 3. - Continued. Variation of pressure coefficient with angle of attack at each orifice station.

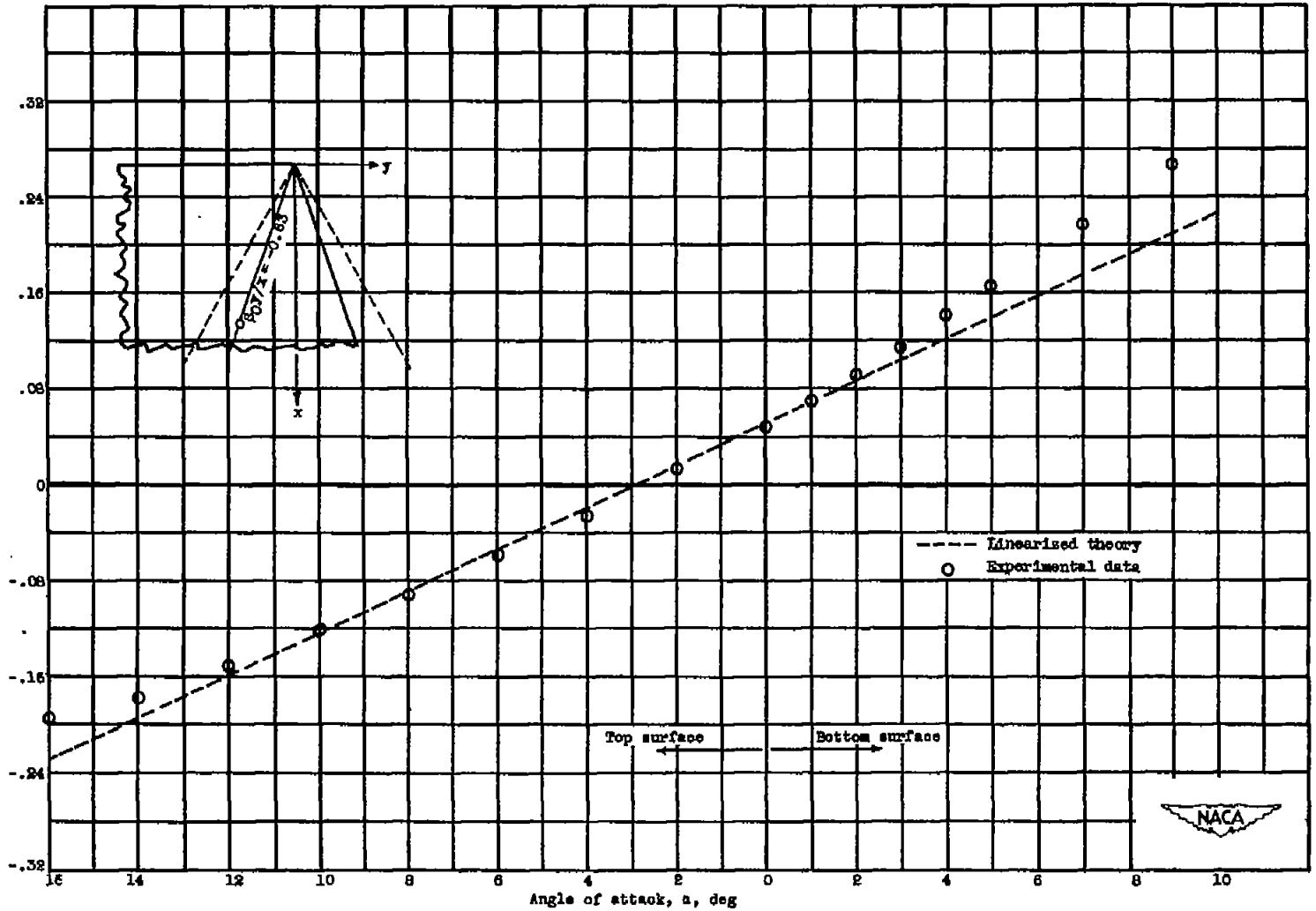

(e) $\beta_0 y/x = -0.65$.

Figure 5. - Continued. Variation of pressure coefficient with angle of attack at each orifice station.

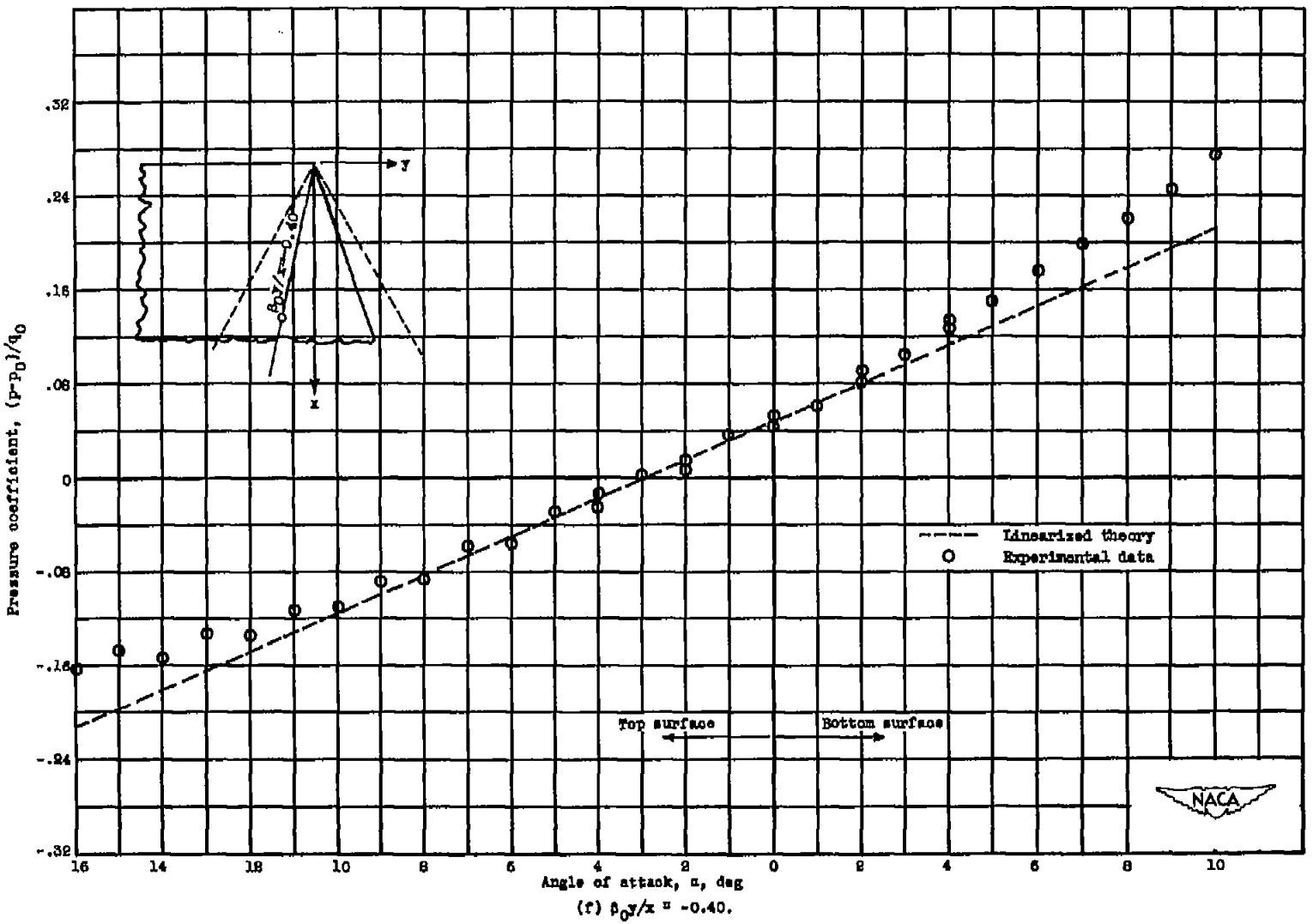

(f) $\beta_0 y/x = -0.40$.

Figure 3. - Continued. Variation of pressure coefficient with angle of attack of each orifice station.

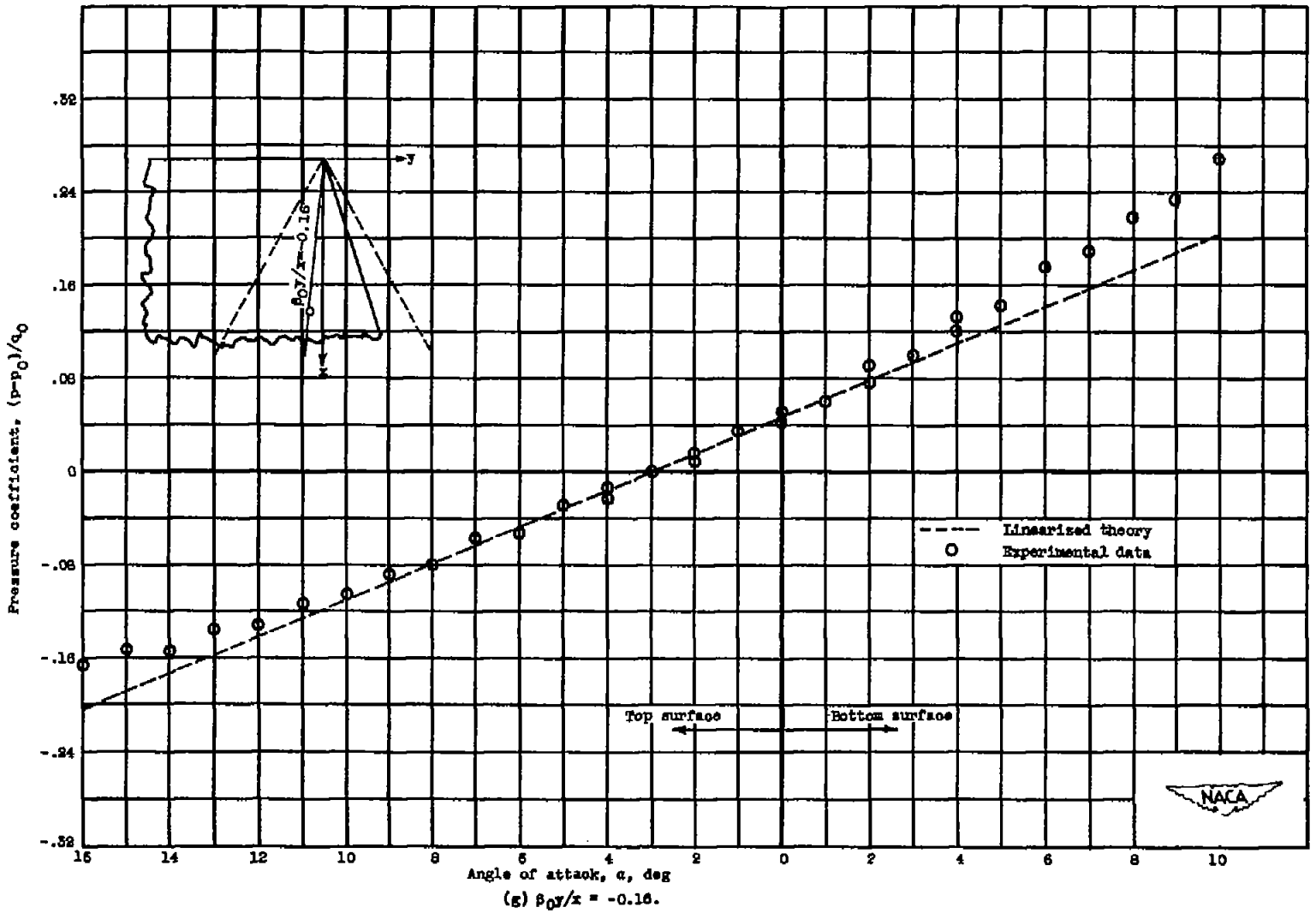

(g) $\beta_0 y/x = -0.16$.

Figure 5. - Continued. Variation of pressure coefficient with angle of attack at each orifice station.

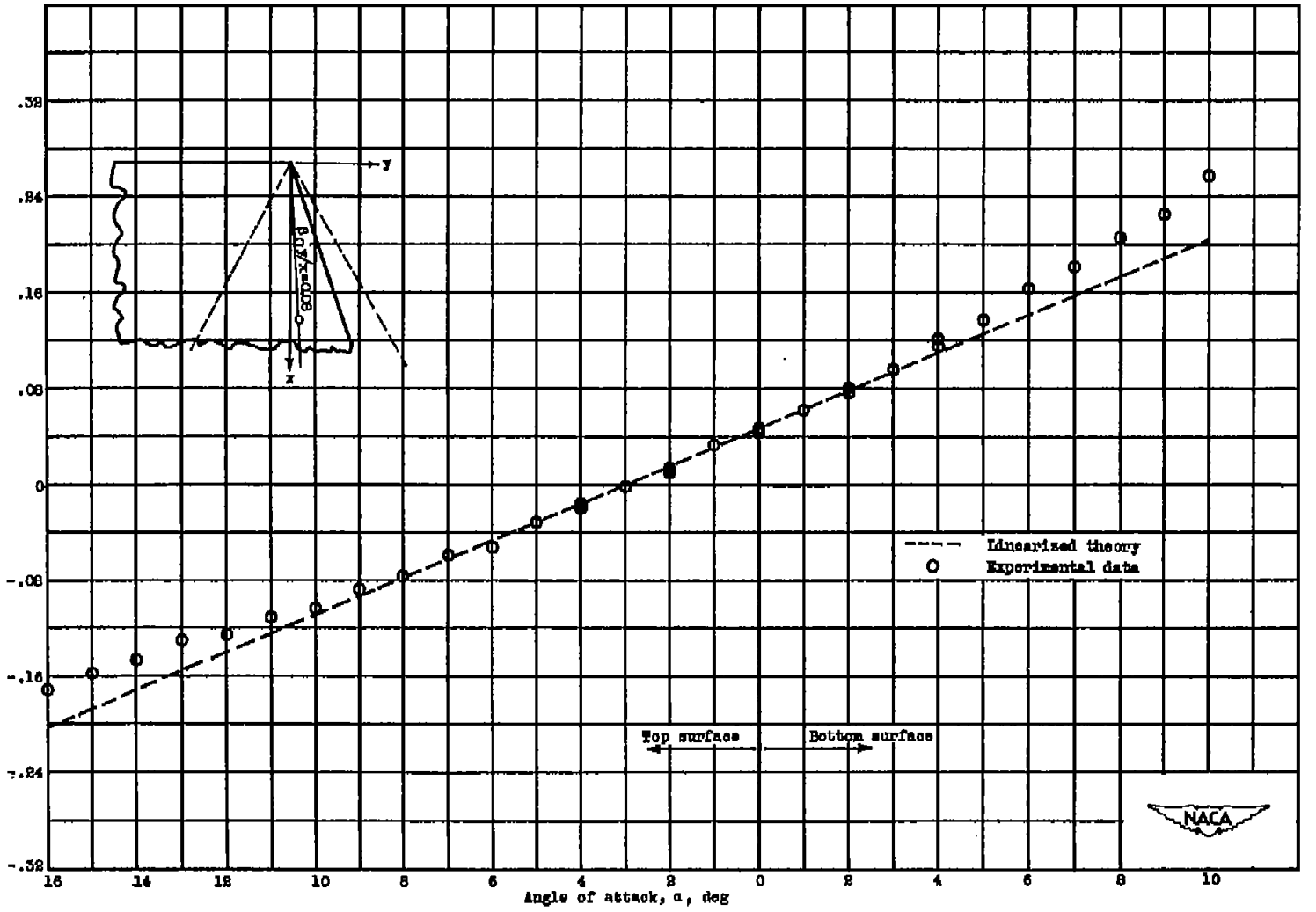

(h) $\beta_0 y/x = 0.08$.

Figure 5. - Continued. Variation of pressure coefficient with angle of attack at each orifice station.

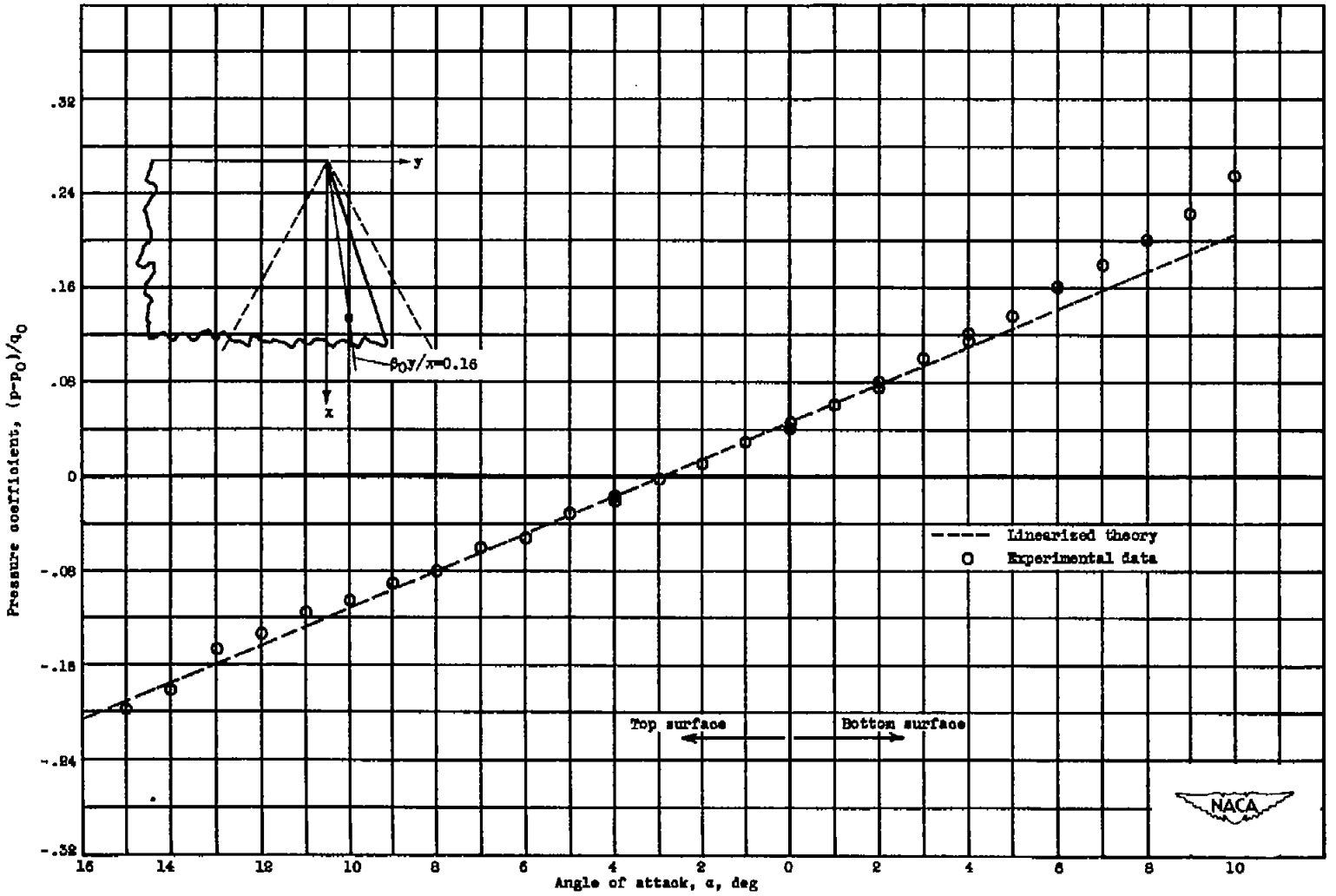

(l) $\beta_0 y/x = 0.16$.

Figure 3. - Continued. Variation of pressure coefficient with angle of attack at each orifice station.

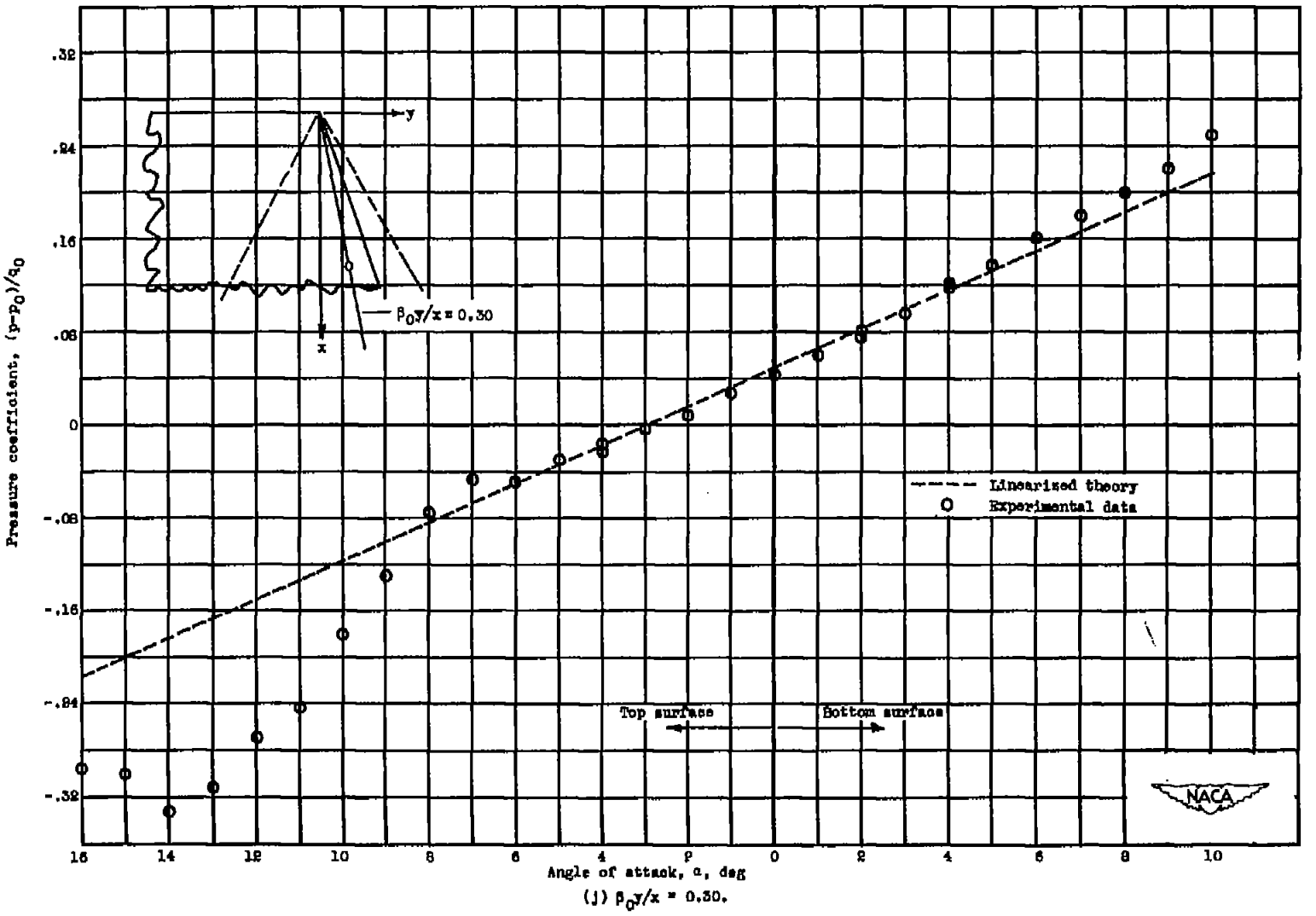

(j) $\beta_0 y/x = 0.30$.

Figure 3. - Continued. Variation of pressure coefficient with angle of attack of each orifice station.

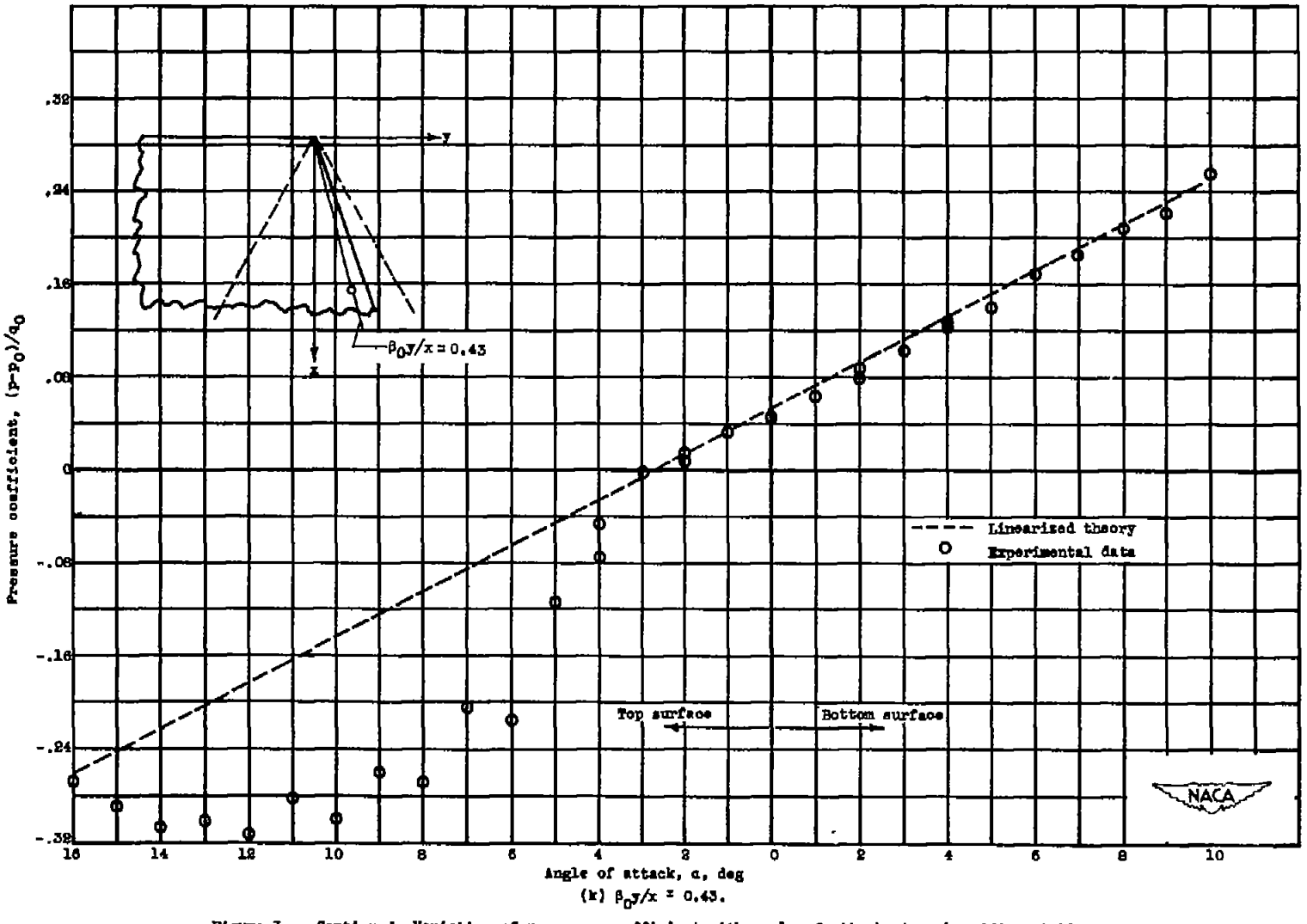

(k) $\beta_0 y/x = 0.43$.

Figure 3. - Continued. Variation of pressure coefficient with angle of attack at each orifice station.

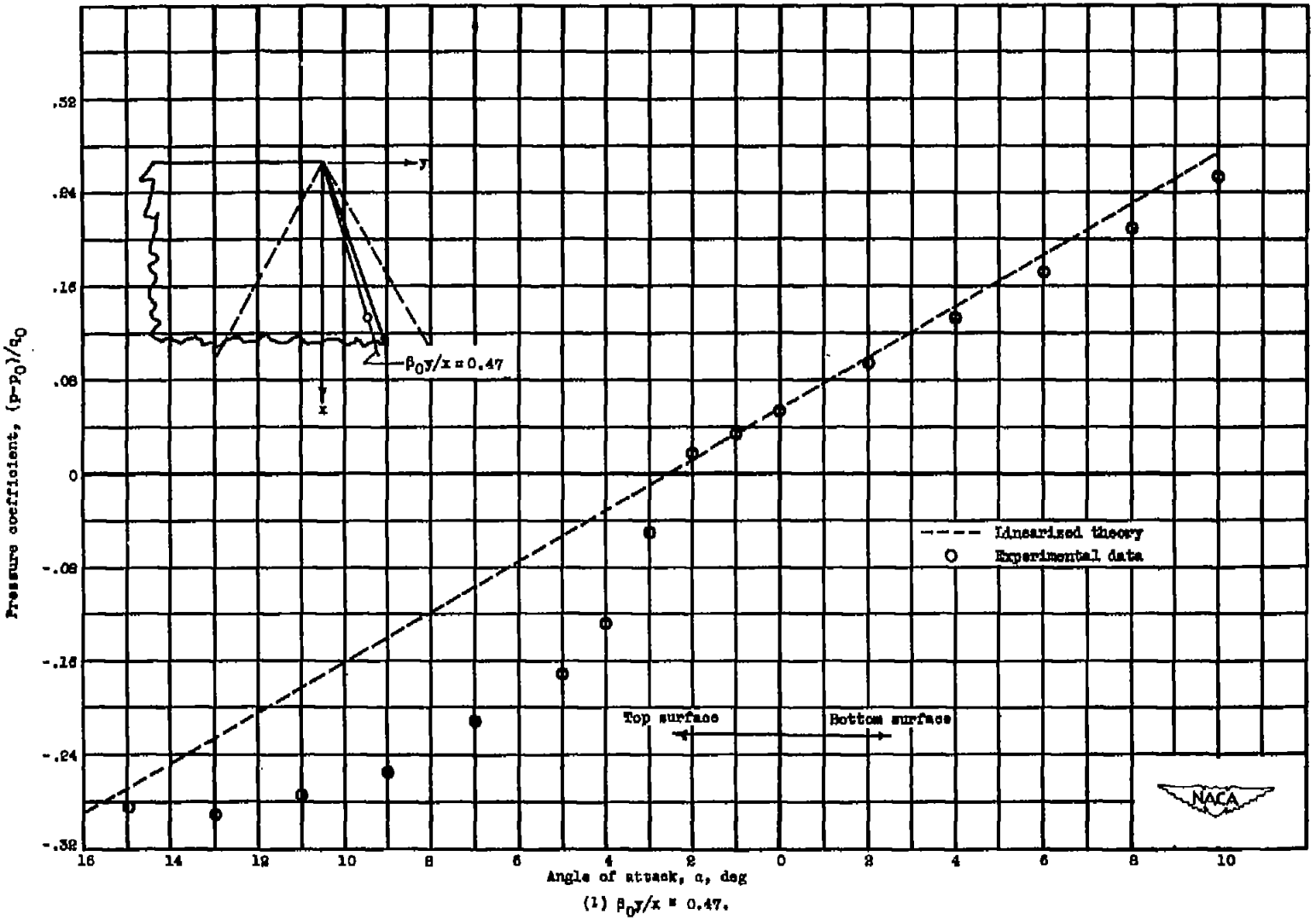

(1) $\beta_0 y/x = 0.47$.

Figure 5. - Concluded. Variation of pressure coefficient with angle of attack at each orifice station.

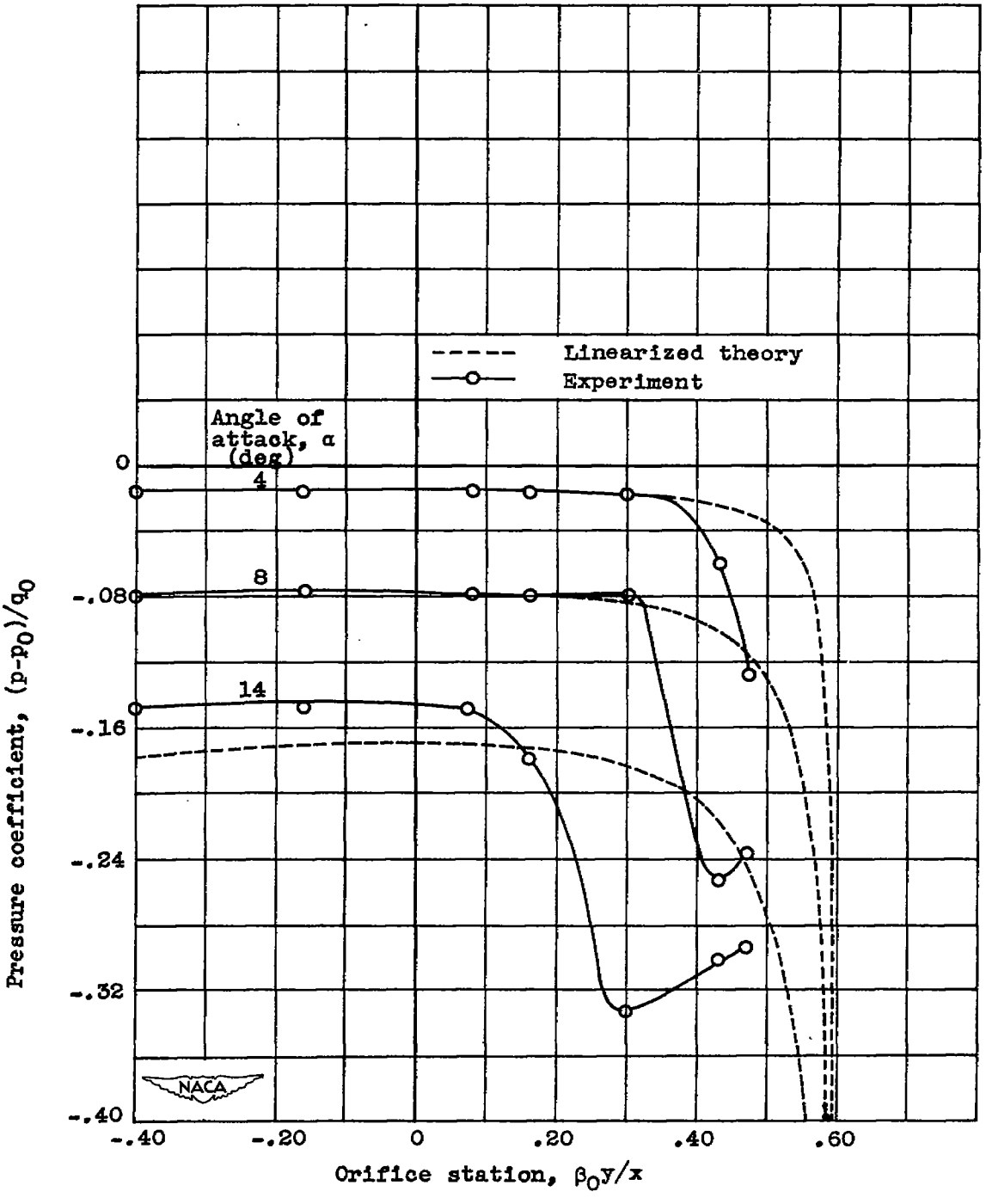

Figure 4. - Pressure coefficients on top surface in vicinity of subsonic leading edge.

[redacted]

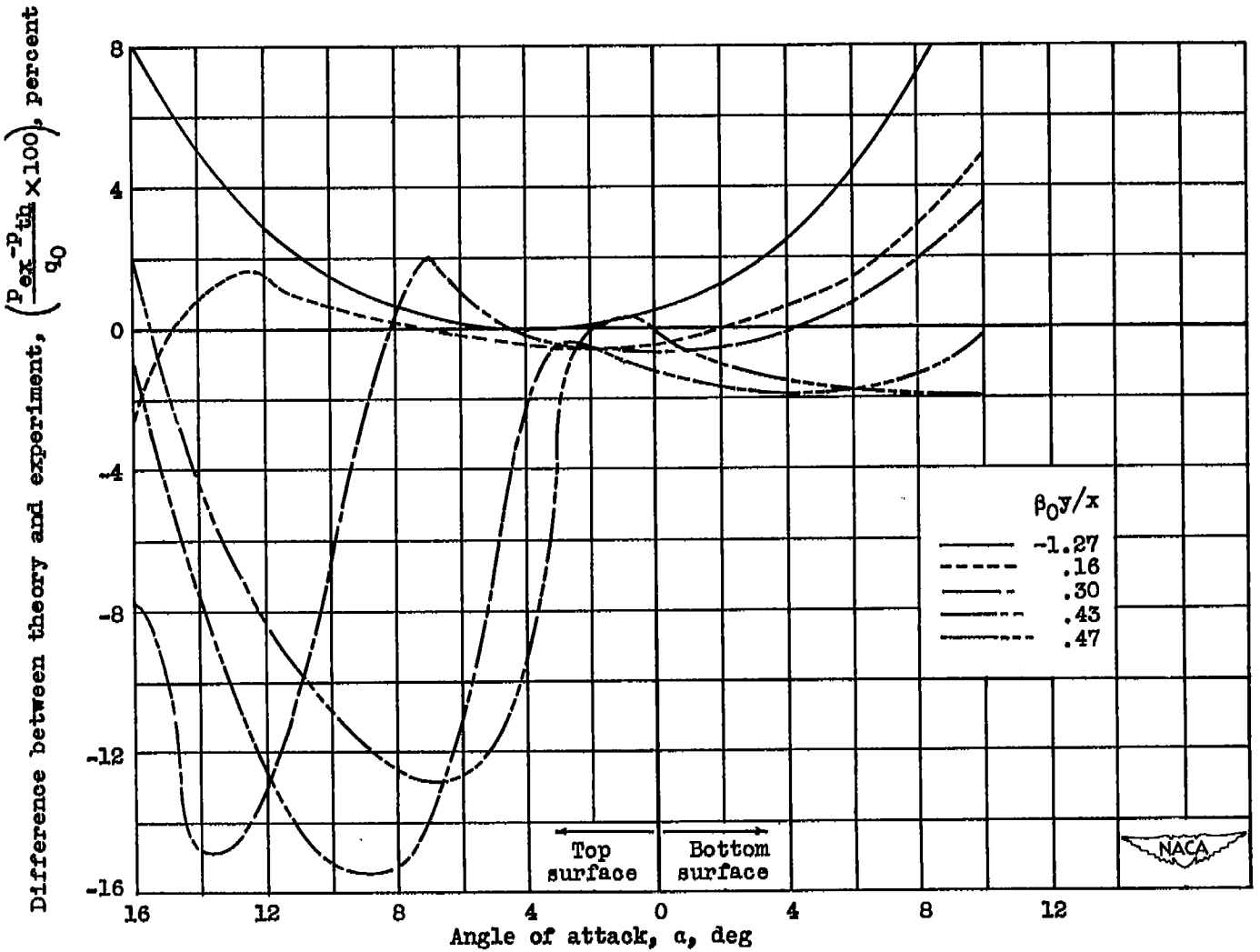

Figure 5. - Difference between experimental data and linearized theory in percentage of free-stream dynamic pressure.

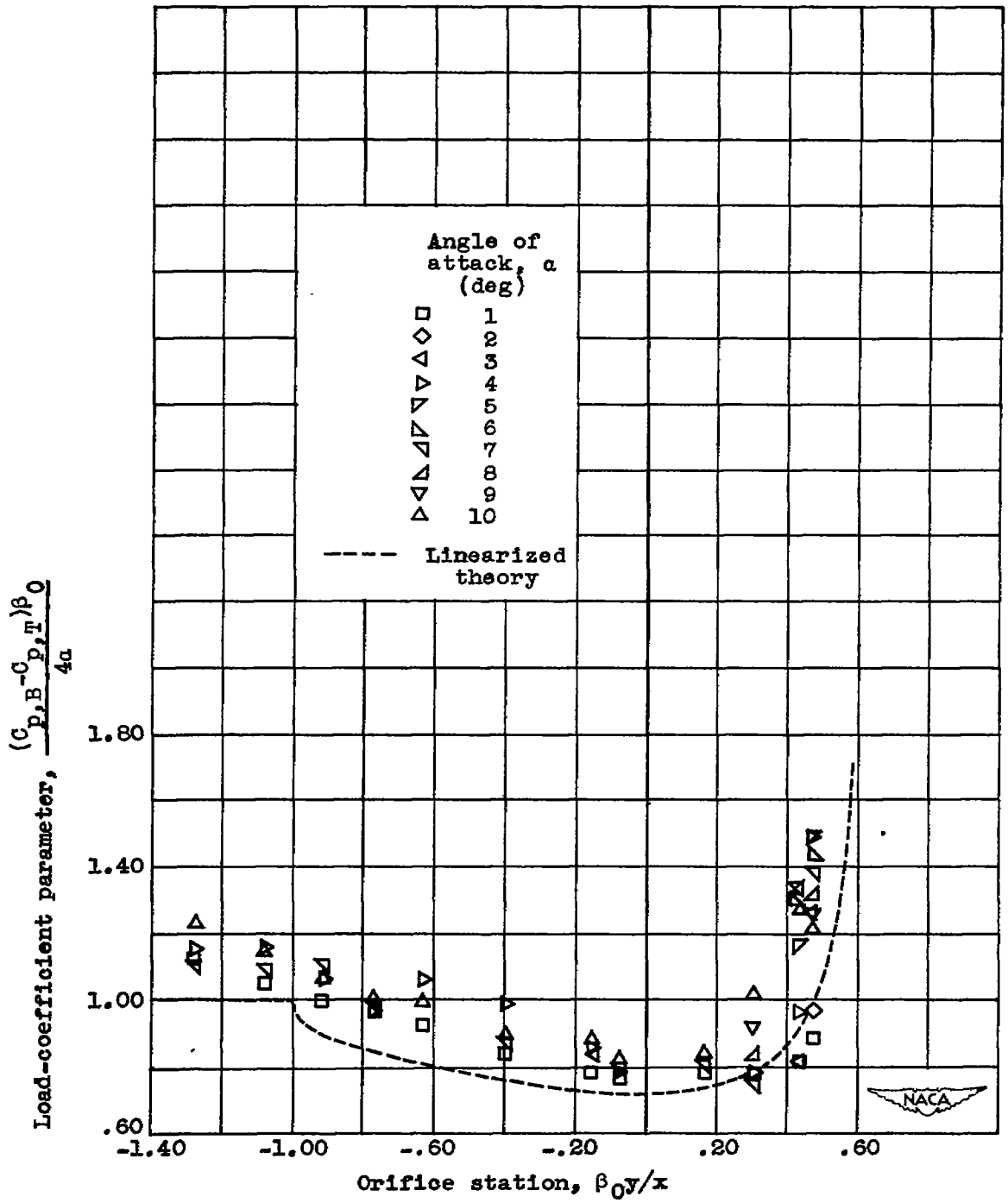

Figure 6. - Comparison of observed and theoretical load distribution.

[redacted]